
Article:
Malica, Tushar, Panajotov, Krassimir, Avrutin, Evgeny orcid.org/0000-0001-5488-3222 et al. (1 more author) (2023) Passively mode-locked high-frequency dual-VCSEL system. Optics Express. pp. 8296-8306. ISSN 1094-4087

https://doi.org/10.1364/OE.480388

Research Article Vol. 31, No. 5 / 27 Feb 2023 / Optics Express 8296
Optics EXPRESS

Passively mode-locked high-frequency dual-VCSEL system

TUSHAR MALICA,[1,2,*] KRASSIMIR PANAJOTOV,[3,4] EUGENE A. AVRUTIN,[5] AND MARC SCIAMANNA[1,2]

[1]Chaire Photonique, LMOPS, CentraleSupélec, 2 Rue Edouard Belin 57070 Metz, France
[2]Université de Lorraine, LMOPS, 2 Rue Edouard Belin 57070 Metz, France
[3]Faculty of Engineering Sciences, Brussels Photonics Team B-PHOT, Vrije Universiteit Brussel,1050 Brussels, Belgium
[4]G. Nadjakov Institute of Solid State Physics, Bulgarian Academy of Sciences, 1784 Sofia, Bulgaria
[5]School of Physics, Engineering, and Technology, University of York, York YO10 5DD, UK
[*]tushar.malica@centralesupelec.fr

Abstract: Two VCSELs placed facing each other with one biased chip while the second chip is unbiased is shown as a promising alternative to the popularly used conventional SESAM mode-locked VECSEL to generate mode-locked pulses. We propose a theoretical model using time-delay differential rate equations and numerically show that the proposed dual-laser configuration functions as a typical gain-absorber system. Parameter space defined by laser facet reflectivities and current are used to show general trends in the exhibited nonlinear dynamics and pulsed solutions.

1. Introduction

Vertical-Cavity Surface-Emitting Lasers (VCSELs) were developed over the last two decades of the last century and found a multitude of applications such as optical communications, optical sensing, displays, illuminations, computer optics, mobiles, etc. [1,2]. Despite being highly reflective devices with low gain and much shorter cavity compared to the edge-emitting lasers, VCSELs exhibit a similar richness in nonlinear dynamics [3–6]. VECSELs(Vertical Extended-Cavity Surface-Emitting Lasers), in which one of the reflectors is external to the cavity [7], maintain some of the advantages of fully monolithic VCSELs, such as the circular beam shape, but have very different, dynamics properties (and potentially an extra means of controlling them) due to the long air cavity. Since 2000, semiconductor saturable absorber mirror (SESAM) have been incorporated with VCSELs, both in an external cavity configuration and on-chip, to produce passively modelocked pulses [8–10]. With the advancement of technology in SESAM-modelocked VECSELs have exhibited fundamentally modelocked pulses at repetition frequencies between 85 MHz to 100 GHz [11,12]. While pulse durations as low as 100 fs have been achieved [13]. Almost concurrent, the idea of two mutually coupled semiconductor lasers in face-to-face configuration was explored in [14–16] and further expanded towards VCSELs [17–20]. The present work theoretically shows the possibility of producing modelocked pulses in an external cavity configuration using two VCSELs facing each other. By combining the idea of SESAM-modelocked VECSELs and mutually coupled VCSELs, we show that a VCSEL can replace the function of a SESAM and exhibit a similar range of dynamics with reasonable pulse duration in the several hundred femtoseconds range.

From the perspective of theoretical modelling, mutually-coupled laser systems have been modelled through the delay-differential equations model [14] and composite-cavity modelling based on semi-classical laser theory [21,22]. Specifically, the pulsed operation is modelled in the VECSEL cavities through delay-differential equations as in [23] and the iterative pulse shaping model [24–26]. In the presented work, we modify an existing generic theoretical model

#480388 https://doi.org/10.1364/OE.480388
Journal © 2023 Received 29 Nov 2022; revised 1 Feb 2023; accepted 1 Feb 2023; published 21 Feb 2023

Optics EXPRESS

proposed in [23] based on delay-differential equations to simulate a pair of mutually-coupled VCSEL chips instead of a typical VCSEL-SESAM external cavity configuration. The advantage of employing delay-differential modelling over iterative modelling is the capability of exhibiting both mode-locked and non-pulsed outputs without encountering the issue of stiff differential equations. It should be noted that the iterative modelling has been used to successfully verify mode-locked outputs upon feeding precise experimentally measured parameters [25]. However, the proposed model here is used for the prediction of dynamics rather than for verification of the experimental data. It is not limited to the prediction of pulsed states and is capable of exhibiting chaotic and/or non-pulsed outputs. Furthermore, the model operates on user-defined realistic experimental parameter values like cavity length, bias current, laser facet reflectivities etc. enabling direct comparison to experiments which cater to the demands of integrated photonic device makers.

The intention to develop and pursue this line of investigation is to primarily understand the possibility and parameter space mapping of generating mode-locked pulses with two mutually coupled VCSELs. Our work predicts the capability of such a system to generate mode-locked pulses of picosecond and femtosecond regimes. Such results, comparable to typical SESAM modelocked VECSELs, are promising and can provide a decent alternative for general applications or even serve as an origin for pre-compressed pulses in applications where the source of mode-locked pulses is not important. Finally, selecting such an alternative also lowers the exercise of designing the laser, engineering of SESAM, and its associated cost.

2. Theoretical model

Two single-longitudinal mode VCSELs are considered as shown in Fig. 1. The VCSEL functioning as the gain element is biased, while the second VCSEL is unbiased, thereby acting as the absorber. The parameters associated with the VCSELs functioning as the gain and the absorber are referred to using subscripts 'g'and 'a', respectively, from here onwards. Table 1 shows the list of two VCSELs' parameters and their values mainly based on [23]. The front mirror reflectance of the gain chip is reduced from ≈ 1 to as low as 0.7 systematically while the reflectances of the absorber chip are varied between ≈ 1 to 0.1 to report the observed dynamics and displayed as parameter space region plots. The two chips are treated as resonators, so the reflectance from the front mirror is automatically included within the feedback terms. Furthermore, the VCSELs acting as the gain and the absorber with lower reflectances are not the same as the ones employed in a traditional SESAM modelocked VCSEL model. For example, the VCSEL chip used here has a higher reflectance facing the cavity and is somewhat lower than a free-standing VCSEL, along with a slower recovery time than a normal SESAM.

The delay-differential equation model used to calculate carrier density and electric fields is based on the formalism introduced in [23]. The carrier density rate equations are formulated as follows:

$$\frac{dN_{g,a}}{dt} = \frac{I_{g,a}}{ed_{g,a}} - \frac{N_{g,a}}{\tau_{g,a}} - v_{g,a}[G_{ng,na}\{N_{g,a}(t) - N_{trg,a}\}]S_{g,a} \tag{1}$$

where $I_a = 0$. The gain suppression is assumed to be zero, and the carrier lifetime to be constant and independent of carrier density. Non-equilibrium carrier effects, as recently studied by a fully microscopic many-body model for the carrier distributions and polarizations in [27], are important for femtosecond operation, and may violate the assumptions above are not considered. The gain is assumed to be linear and stated on the R.H.S. of Eq. (1) within the square brackets. The group velocity is calculated as $v_{g,a} = c/n_{g,a}$, with c being the typical value for the speed of light. The photon density is defined as:

$$S_{g,a} = \left|\left(\frac{1 + r_{og,a}}{t_{ig,a}}\right)E_{rcg,a}\right|^2, \tag{2}$$

Optics EXPRESS

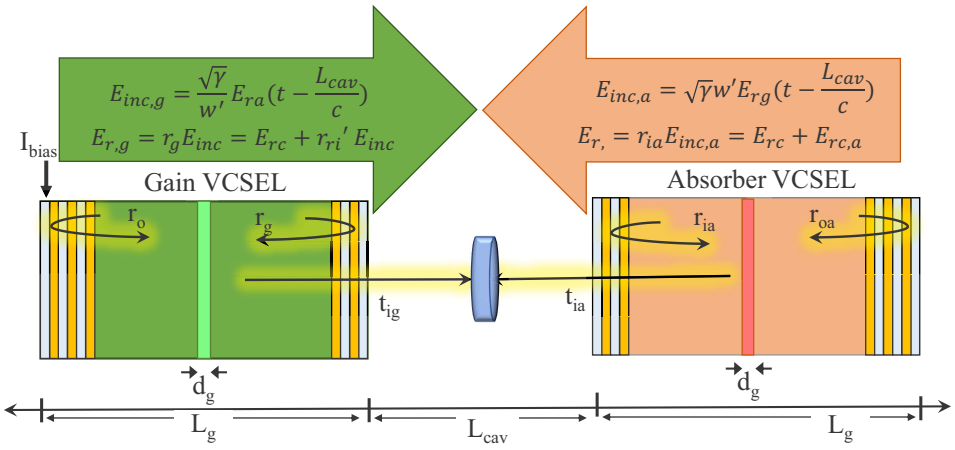

Fig. 1. Schematic representation of a dual-VCSEL configuration with one laser acting as the gain biased at current set to I_{bias} while the second laser (the absorber) is unbiased. The external cavity length is shown by L_{cav}, $E_{inc,g(a)}$ denotes the complex amplitude of the incident fields, $E_{rc,g(a)}$ represents the complex amplitude of the field exiting the respective chip into the external cavity and the laser parameters are stated in Table 1

Table 1. VCSEL gain and absorber chip parameters

Parameter	Value
Back mirror amplitude reflectivity of the gain (r_o)	0.9995
Back mirror amplitude reflectivity of the absorber ($r_o a$)	0.97
Group refractive index($n_{g,a}$)	3.5
Internal losses for both chips (α_i)	0.001 μm^{-1}
Effective length for both chips (L_g)	1.5 μm
Quantum cumulative thickness for both chips (d_g)	0.024 μm
Radius of the active region for both chips (ρ_g)	1.2 μm
Group refractive index for both chips (n_{rg})	3.5
Confinement factor for both chips (Γ_g)	0.06
Linewidth enhancement factor for both chips (α_g)	3
Carrier lifetime for the gain chip (τ_g)	1 ns
Carrier lifetime for the absorber chip (τ_a)	0.1 ns
Transparency carrier density of the gain (N_{tr})	$1 \times 10^6 \mu m^{-3}$
Transparency carrier density of the absorber (N_{tr})	$2 \times 10^6 \mu m^{-3}$
Gain coefficient of the gain (G_n)	$7 \times 10^{-8} \mu m^{-1}$
Gain coefficient of the absorber (G_n)	$2.5 \times 10^{-7} \mu m^{-1}$
Inter-chip attenuation for both chips (γ)	1
Beam cross-section diameter ratio (gain:absorber) (w')	2
External cavity round-trip time (τ_{RT})	0.08 ns

where $E_{rcg,a}$ is the field reflected from the respective VCSEL chips. It is calculated by [23]:

$$\tau_{g,a}\theta_{cg,a}\frac{dE_{rcg,a}}{dt} = [\delta\tilde{G}_{g,a} - (1-\theta_{cg,a})]E_{rcg,a} + t_{ig,a}t'_i r_{og,a} e^{-\alpha_{ig,a}L_{cg,a}}\left[\frac{\sqrt{\gamma_{g,a}}}{w'_{g,a}}E_r^{(g,a)}(t-\tau_{cav})\right], \quad (3)$$

Optics EXPRESS

where $E_{incg,a}$ is a complex field of the incident field as stated within the square brackets on the R.H.S. of Eq. (3). The real cavity attenuation factor is calculated as $\theta_{cg,a} = r_{ig,a} r_{og,a} e^{-\alpha_i L}$, and L is the geometric cavity length of the gain and the absorber chips. The transmissivity factors ($t_{ig,a}$) are calculated using the standard formula of $t_{ig,a} = \sqrt{1 - r_{ig,a}^2}$, in accordance with Fresnel equations to maintain the sum of the reflectance and the transmittance at the media interface equal to unity. Similarly, $t_i^{'}$ is the transmittance seen by the light exiting from the laser facet mirror towards the external cavity side, which has the same amplitude as r_g, but with a different phase. The parameters entering Eqns. 1–3 and their values are listed in Table 1.

As discussed in [23], the model as described using Eqns. 1–3 does account for the cavity bandwidths of the gain and absorber VCSEL chips; however, it contains several important limitations. Most importantly, the dispersion of the gain (in the gain chip) and absorption (in the absorber chip), and associated group dispersion delay, are neglected. Secondly, it is assumed that the resonant frequencies of the gain and absorber chips are identical. Finally, we note that the assumption related to a zero gain suppression and the linear gain trend should not change the dynamics qualitatively. Specifically, it is known that the shape of the pulse is regulated by the interaction between gain and absorption coefficients and that a resultant positive gain gives rise to a pulse inside the external cavity [9]. This does not necessarily need be at the gain maximum. Competition between these two mechanisms regulates the leading and the trailing edges of a pulse. The pulses will broaden if the gain compression dominates, while the pulse shortens and the area of stable mode-locking broadens if the absorption suppression dominates [9,10]. Thus, the effect on pulse dynamics will depend on the relation between gain and absorption compression coefficients. While the order of magnitude of the two coefficients is reasonably well known, the relation between them is not easy to determine from the literature. Calculating them from the first principles would be a separate, nontrivial study. Therefore, in this initial work, we assume that they cancel each other effectively.

3. Results and discussion

Figure 2 shows samples of system outputs that reflect qualitatively different dynamics, which are later mapped in the parameter space in Figs. 4–6. Generally speaking, there is persistent Fundamental Mode Locking (FML) in the system over the majority of the parameter space region corresponding to stable pulse emission at the repetition frequency corresponding to the external cavity round-trip (τ_{RT} = 0.08 ns unless specified otherwise). Initially, the instability in the system is manifested in the FML pulse (fig. 2(a)) initially as a small shoulder pulse creeping into the system output accompanied by amplitude modulation. This leads to pulse splitting as seen in fig. 2(b) and followed by fig. 2(c). At higher current values and increasing nonlinearity, we observe chaotic repetitive dynamics as shown in fig. 2(d). Figure 3 shows a typical optical spectrum observed for fundamentally mode-locked pulses. The spectrum shown here is for the same parameters generating pulses as seen in Fig. 2(a).

Figures 4–6 show the general trend in the system dynamics for the parameter space defined by the absorber's inner reflectivity and the bias current applied to the gain chip. The inner reflectivity of the gain chip is increased in each plot to observe the varying dynamics within the same set of operating conditions. The variety of dynamics is indicated by different colours as indicated in the caption. The focus of this study is to report the FML region; therefore, non-pulsed dynamics or multi-pulsation is reported but will not be analyzed in detail. Remarkably, there are always large green regions where FML is stable. Furthermore, we observe that the region of FML shrinks and moves to higher absorber reflectivity as the reflectivity of the gain chip is increased. Simultaneously, the blue region with mode-locked operation with a secondary pulse and the hatched green region of multiple-pulse operation become enlarged. The same concerns the red region in which the system exhibits chaotic dynamics. The threshold current at which lasing

Optics EXPRESS

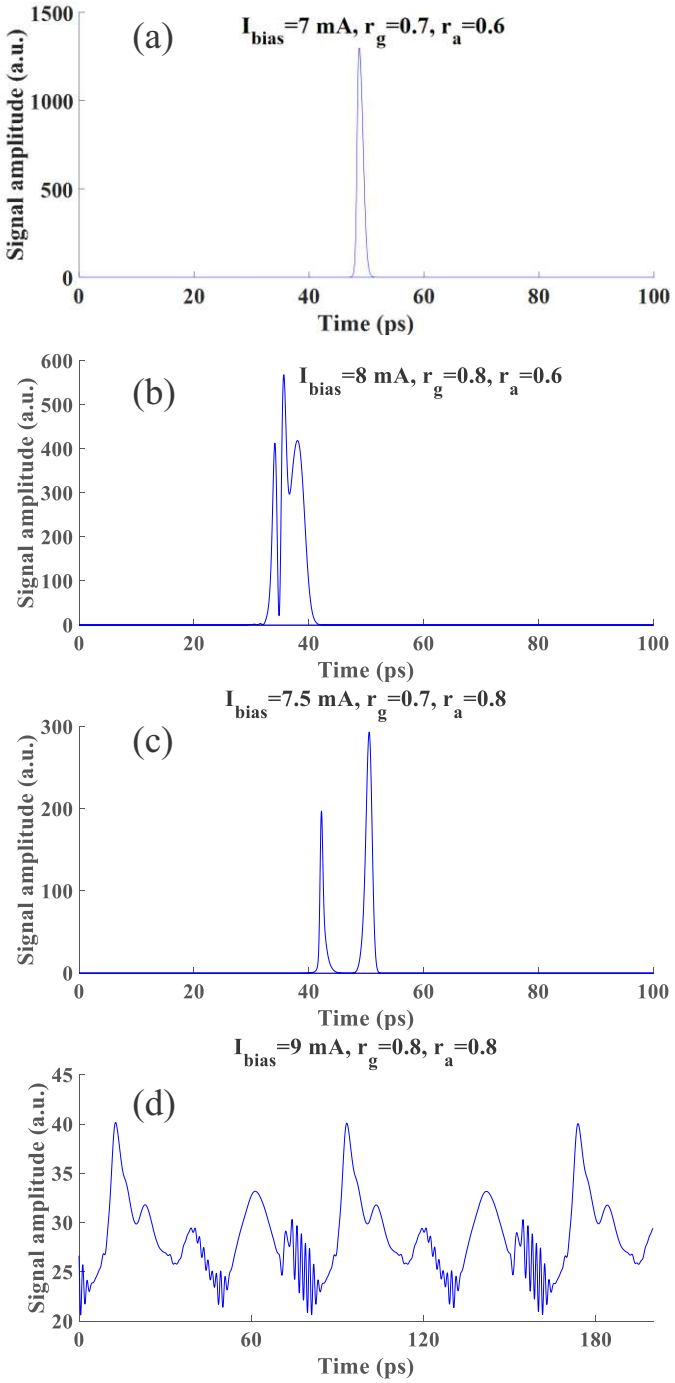

Fig. 2. Samples of system outputs for $\tau_{RT} = 0.08$ ns: (a)Fundamental mode-locked pulse, (b) Pulse splitting, (c) Double pulsing, (d) Chaotic dynamics

Optics EXPRESS

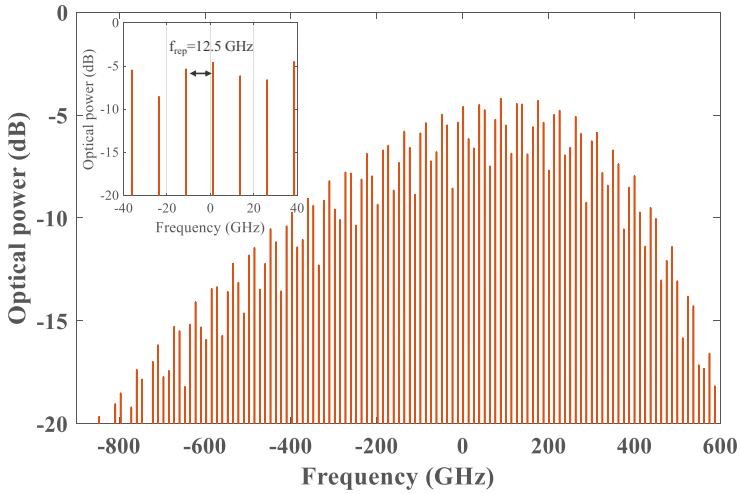

Fig. 3. Optical spectrum calculated using Fast Fourier Transform for Fig. 2(a) showing locked longitudinal modes at a repetition rate f_{rep}= 12.5 GHz. Inset: Magnified subset of the optical spectrum to show the mode-locking.

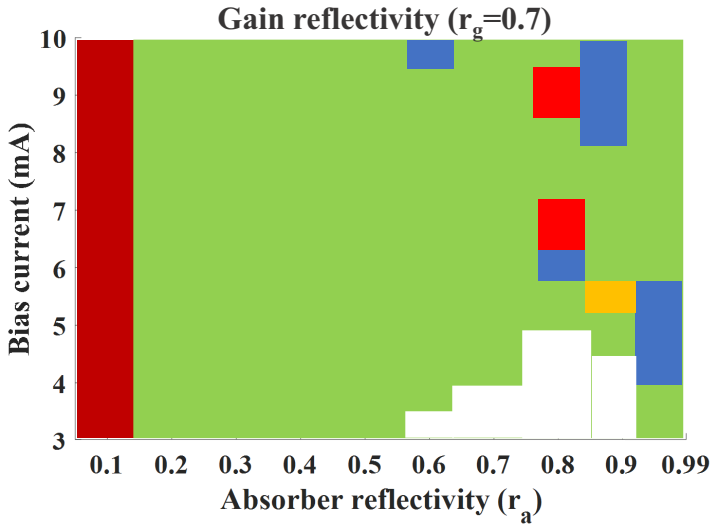

Fig. 4. Dynamical mapping for τ_{RT} = 0.08 ns and r_g=0.7. Green: FML; Green (hatched): FML with amplitude modulation; Blue: FML with shoulder pulse; Orange: Double pulsing; Yellow: Double pulsing with shoulder pulse; Red: Fast chaotic dynamics.

begins increases at higher values of absorber reflectivity. The same trend for threshold current is also observed as the value of gain reflectivity is increased.

Particularly focussing on FML region across Figs. 4–6, we show the dynamics traversing away from FML in Fig. 7. To produce this figure, we keep the absorber's reflectivity constant at 0.7, as observed in Figs. 4–6 and vary the gain chip reflectivity while plotting the local maxima (indicated in red markers) and local minima (indicated in blue markers). The FML region is observed to be limited to lower values of bias current as the gain chip's reflectivity increases from r_g =0.7 in Fig. 7(a) to r_g =0.9 in Fig. 7(c). Furthermore, the pulse peak intensity reduces

Optics EXPRESS

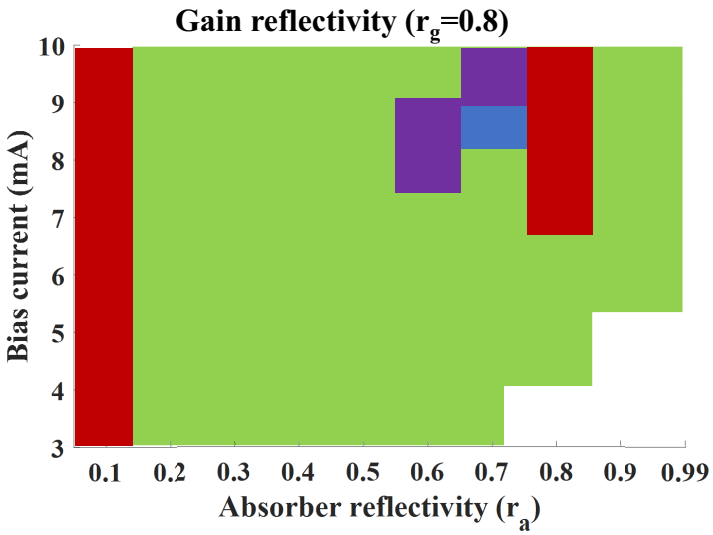

Fig. 5. Dynamical mapping for τ_{RT} = 0.08 ns and r_g=0.8.Green: FML; Green (hatched): FML with amplitude modulation; Blue: FML with shoulder pulse; Red: Fast chaotic dynamics; Purple: Pulse splitting.

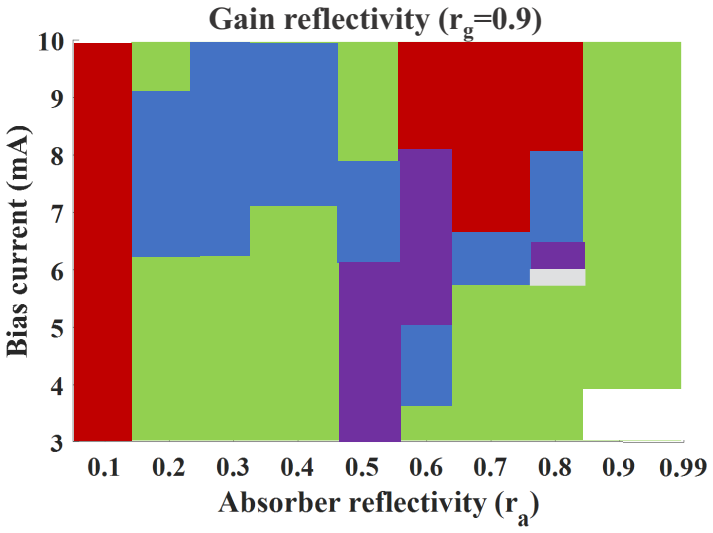

Fig. 6. Dynamical mapping for τ_{RT} = 0.08 ns and r_g=0.9.Green: FML; Green (hatched): FML with amplitude modulation; Blue: FML with shoulder pulse; Red: Fast chaotic dynamics; Purple: Pulse splitting; Grey: Harmonic mode-locking.

significantly as well. For higher bias currents, non-FML and complex dynamics show local maxima and minima unevenly distributed as expected. Additionally, the gap between the values of maxima and minima closes as well.

We also note that the stability of fundamental mode-locking is disturbed as one increases the cavity length, as seen in Fig. 8. We observe clean FML pulses until τ_{RT} =0.4 ns. However, there is some minor pulse splitting at the peak of the pulses, as seen by local maxima and minima coinciding for τ_{RT} = 0.24 ns and τ_{RT} = 0.32 ns. At even longer cavity lengths, we observe

Optics EXPRESS

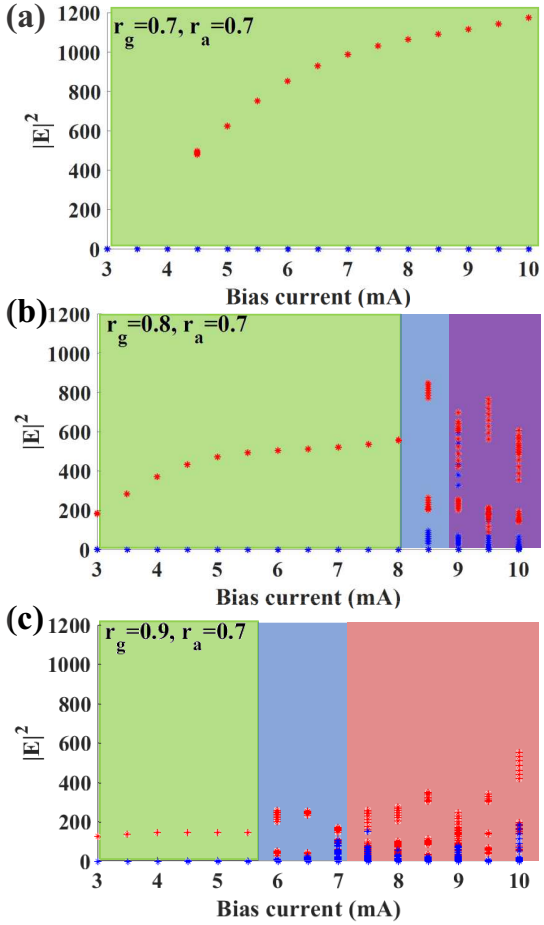

Fig. 7. Local maxima (red) and local minima (blue) as a function of bias current (mA) for r_a = 0.7 and increasing r_g (a) 0.7, (b) 0.8, (c) 0.9. The background shades are reflective of the key indicated in the caption of the Figs. 4–6 namely, blue: FML with shoulder pulse; red: fast chaotic dynamics and purple: pulse splitting.

consistent amplitude modulation and pulse splitting. On the other hand, the peak pulse intensity can also be observed to have increased. It should be noted that the computation time increases with an increase in the cavity length.

Figure 9 shows the average pulse durations at constant absorber reflectivity values across the range of bias currents and a variety of gain chip inner reflectivity. The pulse duration increases at a constant bias current with increasing the gain chip reflectivity. The pulse duration almost doubles for very high gain chip reflectivity (r_g>0.9). This broadening of the pulses is also synchronous with the increase in the parameter space occupied by complex and non-FML dynamics in Fig. 6 compared to Figs. 4 and 5.

On the other hand, no general trend is observed in Fig. 10, when keeping the bias current constant and observing the pulse durations with changing absorber reflectivity for a variety of gain chip reflectivity. It should be noted that the pulse durations observed as low as 60 fs are indeed the current limit of state-of-the-art fundamental modelocked pulses [28]. However, pulse durations below 100 fs are predicted in Figs. 9 and 10 need a more detailed study of the possibility of such short pulse generation in our dual VCSEL system. It is certainly limited by the

Optics EXPRESS

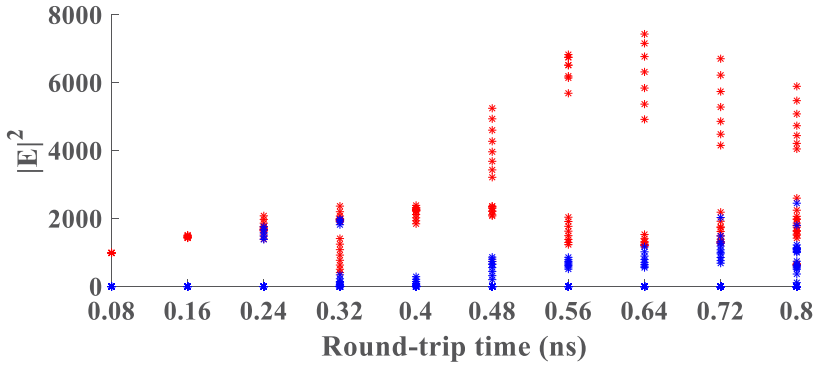

Fig. 8. Instability in FML output via pulse splits and amplitude modulation shown using local maxima (red) and local minima (blue) as a function of round-trip time at $r_g = r_a = 0.7$, $I_{bias} = 7$ mA.

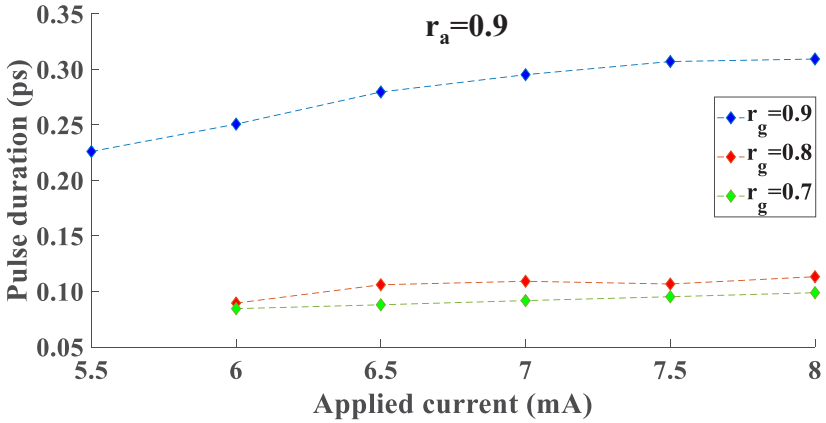

Fig. 9. FML Pulse duration (ps) as a function of bias current at constant r_a=0.9

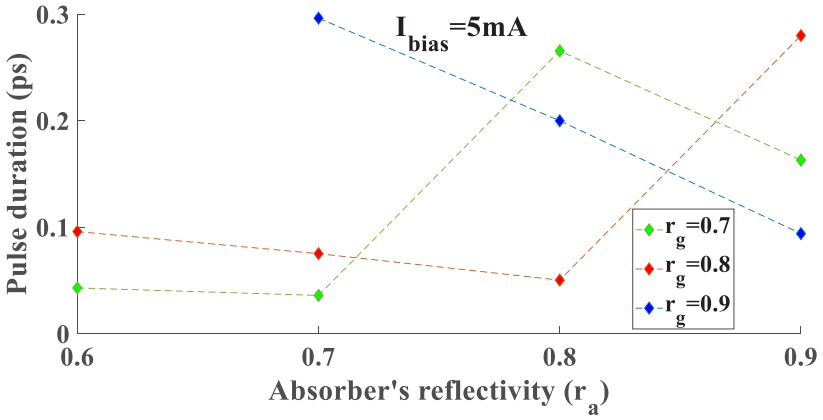

Fig. 10. FML Pulse duration (ps) as a function of r_a at a constant bias current

Optics EXPRESS

VCSEL chip parameters, such as the inner side reflectances of the laser diode chips, and needs a shorter absorber recovery time. Additionally, generating such shorter pulses makes it necessary to account more accurately for dispersion and gain and cavities bandwidths. Specifically, the gain and absorption dispersion, with the peak gain detuned dynamically from the cavity resonance and their interplay with the cavity dispersion, need to be analyzed as mentioned above. Fast gain and absorption compression would also need to be taken into consideration. This is reserved for future work.

4. Conclusion

A theoretical model serving as a paradigm for multi-sectional and free-space elements with flexible cavity configuration used to analyze dynamics of mutually-coupled VCSELs chips is shown. It is adapted from the theoretical model proposed in [23], which serves as a foundation for the work done in this study. The model uses experimental parameters as user-defined inputs allowing for direct comparisons to experiments and directed toward the community of photonic device makers. The presented work focuses on studying the parameter space region of mode-locking in a GHz range dual-vcsel chip configuration. The model maps different pulsed and non-pulsed dynamics for a large range of parameters. By studying the defined parameter space region, we show the change in the FML region with a change in the front mirror laser reflectivities. We show the optimal range of parameters exhibiting FML and its instability with changes in cavity lengths. Through this work, we wish to share the proposed theoretical model with the community of integrated photonic device makers and intend to confirm the predictions experimentally in future works.

Funding. Region Grand Est; Eurometropole Metz; Moselle Department; European Regional Development Fund; Ministère de l'Enseignement supérieur, de la Recherche et de l'Innovation; GDI simulation; Methusalem foundation; Fonds Wetenschappelijk Onderzoek (G0E5819N).

Disclosures. The authors declare no conflicts of interest.

Data availability. Data generated or analyzed in the presented research is available upon reasonable request sent to the email address of the corresponding author.

References

1. K. Iga, "Surface-emitting laser—its birth and generation of new optoelectronics field," IEEE J. Sel. Top. Quantum Electron. **6**(6), 1201–1215 (2000).
2. e. R. Michalzik, *VCSELs*, vol. 166 (Springer Series in Optical Sciences, 2013).
3. A. Hsu, J.-F. Seurin, S. Chuang, and K. Choquette, "Optical feedback in vertical-cavity surface-emitting lasers," IEEE J. Quantum Electron. **37**(12), 1643–1649 (2001).
4. C. Quay, I. Maxwell, and J. Hudgings, "Coherence collapse and redshifting in vertical-cavity surface-emitting lasers exposed to strong optical feedback," J. Appl. Phys. **90**(12), 5856–5858 (2001).
5. M. Sciamanna, K. Panajotov, H. Thienpont, I. Veretennicoff, P. Mégret, and M. Blondel, "Optical feedback induces polarization mode hopping in vertical-cavity surface-emitting lasers," Opt. Lett. **28**(17), 1543–1545 (2003).
6. M. Sondermann, H. Bohnet, and T. Ackemann, "Low-frequency fluctuations and polarization dynamics in vertical-cavity surface-emitting lasers with isotropic feedback," Phys. Rev. A **67**(2), 021802 (2003).
7. M. Kuznetsov, F. Hakimi, R. Sprague, and A. Mooradian, "High-power (> 0.5-w cw) diode-pumped vertical-external-cavity surface-emitting semiconductor lasers with circular tem/sub 00/beams," IEEE Photonics Technol. Lett. **9**(8), 1063–1065 (1997).
8. U. Keller, "Recent developments in compact ultrafast lasers," Nature **424**(6950), 831–838 (2003).
9. U. Keller and A. C. Tropper, "Passively modelocked surface-emitting semiconductor lasers," Phys. Rep. **429**(2), 67–120 (2006).
10. M. Guina, A. Rantamäki, and A. Härkönen, "Optically pumped vecsels: review of technology and progress," J. Phys. D: Appl. Phys. **50**(38), 383001 (2017).
11. M. Butkus, E. Viktorov, T. Erneux, C. Hamilton, G. Maker, G. Malcolm, and E. Rafailov, "85.7 mhz repetition rate mode-locked semiconductor disk laser: fundamental and soliton bound states," Opt. Express **21**(21), 25526–25531 (2013).
12. M. Mangold, C. A. Zaugg, S. M. Link, M. Golling, B. W. Tilma, and U. Keller, "Pulse repetition rate scaling from 5 to 100 ghz with a high-power semiconductor disk laser," Opt. Express **22**(5), 6099–6107 (2014).
13. D. Waldburger, S. M. Link, M. Mangold, C. G. Alfieri, E. Gini, M. Golling, B. W. Tilma, and U. Keller, "High-power 100 fs semiconductor disk lasers," Optica **3**(8), 844–852 (2016).

Optics EXPRESS

14. J. Javaloyes, P. Mandel, and D. Pieroux, "Dynamical properties of lasers coupled face to face," Phys. Rev. E **67**(3), 036201 (2003).
15. S. Yanchuk, K. R. Schneider, and L. Recke, "Dynamics of two mutually coupled semiconductor lasers: instantaneous coupling limit," Phys. Rev. E **69**(5), 056221 (2004).
16. E. A. Viktorov, A. Yacomotti, and P. Mandel, "Semiconductor lasers coupled face-to-face," J. Opt. B: Quantum Semiclassical Opt. **6**(2), L9–L12 (2004).
17. X. Li, W. Pan, B. Luo, D. Ma, and W. Zhang, "Nonlinear dynamics and localized synchronization in mutually coupled vcsels," Opt. Laser Technol. **39**(4), 875–880 (2007).
18. K. Panajotov, M. Sciamanna, H. Thienpont, and A. Uchida, "Impact of light polarization on chaos synchronization of mutually coupled vcsels," Opt. Lett. **33**(24), 3031–3033 (2008).
19. I. Gatare, M. Sciamanna, and L. A. K. Panajotov, "Influence of polarization mode competition on the synchronization two unidirectionally coupled vertical-cavity surface-emitting lasers," Opt. Lett. **32**(12), 1629–1631 (2007).
20. M. Sciamanna, I. Gatare, and L. A. K. Panajotov, "Polarization synchronization in unidirectionally coupled vertical-cavity surface-emitting lasers with orthogonal optical injection," Phys. Rev. E **75**(5), 056213 (2007).
21. H. Erzgräber, S. Wieczorek, and B. Krauskopf, "Dynamics of two semiconductor lasers coupled by a passive resonator," Phys. Rev. E **81**(5), 056201 (2010).
22. S. Wieczorek and W. W. Chow, "Global view of nonlinear dynamics in coupled-cavity lasers–a bifurcation study," Opt. Commun. **246**(4-6), 471–493 (2005).
23. E. A. Avrutin and K. Panajotov, "Delay-differential-equation modeling of mode-locked vertical-external-cavity surface-emitting lasers in different cavity configurations," Materials **12**(19), 3224 (2019).
24. C. Campanario and E. Avrutin, "An efficient model for dynamic simulation of mode-locked vertical external cavity surface emitting lasers," in *NUSOD'05. Proceedings of the 5th International Conference on Numerical Simulation of Optoelectronic Devices*., (IEEE, 2005), pp. 85–86.
25. M. Hoffmann, O. D. Sieber, D. J. Maas, V. J. Wittwer, M. Golling, T. Südmeyer, and U. Keller, "Experimental verification of soliton-like pulse-shaping mechanisms in passively mode-locked vecsels," Opt. Express **18**(10), 10143–10153 (2010).
26. O. D. Sieber, M. Hoffmann, V. J. Wittwer, M. Mangold, M. Golling, B. W. Tilma, T. Südmeyer, and U. Keller, "Experimentally verified pulse formation model for high-power femtosecond vecsels," Appl. Phys. B **113**(1), 133–145 (2013).
27. J. Hader, M. Scheller, A. Laurain, I. Kilen, C. Baker, J. V. Moloney, and S. W. Koch, "Ultrafast non-equilibrium carrier dynamics in semiconductor laser mode-locking," Semicond. Sci. Technol. **32**(1), 013002 (2017).
28. A. H. Quarterman, K. G. Wilcox, V. Apostolopoulos, Z. Mihoubi, S. P. Elsmere, I. Farrer, D. A. Ritchie, and A. Tropper, "A passively mode-locked external-cavity semiconductor laser emitting 60-fs pulses," Nat. Photonics **3**(12), 729–731 (2009).